A fuel mapping strategy for unsteady injection processes within the representative interactive linear eddy model (RILEM)

Tim Lackmann[1*], Alan Kerstein[2], Michael Oevermann[1]

[1]Chalmers Tekniska Högskola
[2]Consultant

Abstract
This paper presents a fuel mapping strategy for a new regime-independent combustion modeling strategy for non-premixed combustion in which the linear eddy model (LEM) is used as a representative interactive regime-independent turbulent combustion model coupled to a 3D CFD solver. Parameters and boundary conditions that determine the evolution of the LEM are supplied by the 3D CFD calculation and updated at each time step. The LEM is then solved for the corresponding time step, providing the 3D CFD code with an updated composition state.
This initialization strategy for this new representative interactive linear eddy model (RILEM) is tested by simulations of an n-heptane spray, demonstrating the ability of the RILEM to describe spray combustion processes.

Introduction

Many of the combustion models in use today work reasonably well for traditional diesel (non-premixed) or gasoline (premixed) engines. They take advantage of the physical characteristics of different combustion modes (premixed or non-premixed) and are often based on the assumption of fast chemistry, leading to scale separation between the turbulent and chemical time and length scales. As a result, they are usually not applicable to the modeling of combustion modes other than those for which they were designed, so their usefulness as predictive tools for the development of new engine concepts may be limited. Among the most widely used models are flamelet models for premixed and non-premixed combustion, motivated by the assumption of fast chemistry that implies the formation of laminar flame structures embedded in a turbulent flow field. The coupling between turbulence and chemistry in flamelet-type models is usually achieved in a parametric way (e.g. via the scalar dissipation rate in non-premixed combustion or by means of turbulent velocity fluctuations in premixed combustion), which means that there is no direct interaction between chemistry, molecular transport, and turbulence. However, if the chemical time scales are not fast compared to the fastest turbulent time scales (as is the case during low temperature combustion, ignition, and re-ignition), it becomes important to accurately describe the interactions between chemistry, molecular transport, and turbulence in order to obtain realistic results. Other popular classes of combustion models for engine applications involving non-premixed combustion are stirred/partially stirred reactor models and the volume reactor fraction model (VRFM) [3]. In these models the chemistry is directly integrated.
However, these models do not provide a characteristic length or velocity of combustion and therefore cannot predict/model flame structure. Ideally, a predictive combustion model that can handle multi-mode and multi-regime combustion conditions should include the following features [2]:

- specify the interactions between turbulence, chemistry, and molecular transport in a direct (non-parameterized) way,
- provide a closed-form treatment of chemistry and molecular transport,
- preserve structures (flames) that result from the coupling of reaction and diffusion,
- facilitate resolution at all length and time scales, and
- make no assumptions about statistical distributions (i.e. not rely on presumed PDFs).

Existing regime- and mode- independent combustion models are transported PDF models with structure-based mixing models [16] and low-dimensional stochastic models like LES-LEM, in which the linear eddy model of Kerstein [10] is used as a sub-grid model in a large-eddy simulation (LES) [8, 9, 21, 22]. In LES-LEM a one-dimensional representation of the turbulent combustion process is solved in each LES cell by resolving all spatial and temporal scales, as is done in direct numerical simulations. Compared to most other modeling strategies the characteristic modeling aspect in LEM is this fully resolved one-dimensional representation that does not involve sub-grid scale modeling. Due to the direct interaction between turbulent mixing, diffusion and chemical reactions, the model is capable of predicting highly unsteady effects such as extinction and re-ignition without requiring any modification. One disadvantage of the LES-LEM approach is its high computational cost. Large-scale applications therefore require a well-

*Corresponding author: tim.lackmann@chalmers.se
Proceedings of the European Combustion meeting 2015

parallelized environment together with the adoption of chemistry acceleration techniques such as in situ adaptive tabulation (ISAT) or neural network strategies.

Here we present a LEM approach in which we solve only one representative linear-eddy model which represents the whole computational domain. The goal is to formulate a modeling approach that retains the key advantages of a full LES-LEM, namely regime and mode independence, at acceptable computational cost. Our approach does not exhibit all of the properties identified above as being desirable for mode- and regime-independent modeling because it uses a presumed PDF approach and a globally representative model rather than one that is locally regime-independent. The approach has some similarities with the representative interactive flamelet (RIF) approach of Pitsch et al. [19] but features some distinct advantages such as regime independence and intrinsically variable scalar dissipation rates

Mathematical model

The Linear Eddy model

The Linear-Eddy Model was proposed by Kerstein [6] as a scalar mixing model for non-reacting flows and gradually extended to reactive flow in [10]. It has been discussed in detail in the literature [6, 7, 10, 8, 9], and therefore is only briefly mentioned here. The LEM describes turbulent reactive flows in terms of two concurrent processes representing the respective influences of dilatation induced advection, molecular diffusion, chemical reactions, and turbulent transport. The first process is time advancement of the reactive zero-Mach-number equations on a one-dimensional domain [28,29] resolving all spatial and temporal scales. The second process, turbulent transport, is implemented using a stochastic sequence of statistically independent eddy events. In this paper a spherical formulation of the LEM model is used. This formulation enables a consistent representation of the fuel mapping strategy.

RILEM

On the CFD side the standard set of equations for global mass, momentum, and enthalpy and a standard Lagrangian model spray model including single component fuel evaporation are solved. Turbulence is modeled with the standard κ-ε model. To characterize turbulent fuel mixing, additional transport equations for the mixture fraction $\tilde{Z}$ and the variance of the mixture fraction $\widetilde{Z''^2}$ are solved:

$$(1)\quad \frac{\partial(\bar{\rho}\tilde{Z})}{\partial t} + \nabla\left(\bar{\rho}\tilde{u}\tilde{Z}\right) = \nabla\left[\frac{\mu_t}{Sc_t}\nabla\tilde{Z}\right] + \dot{S}_{evap}$$

$$(2)\quad \frac{\partial(\bar{\rho}\widetilde{Z''^2})}{\partial t} + \nabla\left(\bar{\rho}\tilde{u}\widetilde{Z''^2}\right) = \nabla\left[\frac{\mu_t}{Sc_t}\nabla\widetilde{Z''^2}\right] + 2\frac{\mu_t}{Sc_t}(\nabla Z)^2 - \tilde{\chi}$$

Here, $\dot{S}_{evap}$, μ_t, and are respectively the source term due to evaporation, the turbulent viscosity, and the turbulent Schmidt number (that takes a constant value of 0.7).

The scalar dissipation rate $\tilde{\chi}$ is modeled as

$$(3)\quad \tilde{\chi} = c_\chi \frac{\varepsilon}{k}\widetilde{Z''^2}$$

where $c_\chi = 2$. k presents the turbulent kinetic energy and ε the turbulent kinetic dissipation.

The energy budget in our formulation is solved in the form of an equation for the total enthalpy $\tilde{h}$:

$$(4)\quad \frac{\partial\bar{\rho}\tilde{h}}{\partial t} + \nabla\left(\bar{\rho}\tilde{u}\tilde{h}\right) = \frac{d\bar{p}}{dt} - \nabla j + \dot{q}_{evap}$$

where j is the heat flux vector and $\dot{q}_{evap}$ is the enthalpy source due to droplet evaporation, which is provided by the spray model. Viscous heating has been neglected here, which is a reasonable assumption for low Mach-number flow.

After solving the enthalpy equation, the temperature can be calculated via the caloric equation of state:

$$(5)\quad \tilde{h} = \sum_{s=1}^{n}\tilde{Y}_s h_s\left(\tilde{T}\right).$$

Here, h_S denotes the mass-specific enthalpy of species s including the heat of formation and the temperature dependent sensible enthalpy. The Favre-averaged species mass fractions $\tilde{Y}_S$ in each cell of the computational domain are obtained by integrating LEM mass fraction values mapped onto mixture fraction space using a presumed β-PDF for the mixture fraction:

$$(6)\quad \tilde{Y}_S = \int_0^1 P\left(Z, \tilde{Z}, \widetilde{Z''^2}\right) Y_S^{LEM}(Z)\,dZ$$

Here, $Y_S^{LEM}(Z)$ denotes the mass fraction of species s obtained on the representative LEM, which has been mapped onto mixture fraction space. This mapping differs essentially from that in flamelet models: due to the stochastic nature of the LEM, an arbitrary number of different thermodynamic states are possible for a certain mixture fraction value. This variability of states for a fixed mixture fraction partly reflects the inherent variability of scalar dissipation rates within the LEM. The probability density function of the scalar dissipation rate is an input parameter for flamelet models. Here it is an outcome of the solution.

Fig. 2 presents the basic structure of the RILEM code. CFD and representative LEM solutions are time advanced in an alternating way. First the fluid dynamics are calculated for one time step on the CFD side. Afterwards the LEM is supplied with updated variables for the pressure change, characteristic turbulent length and velocity scales, and information about the evaporated fuel mass.

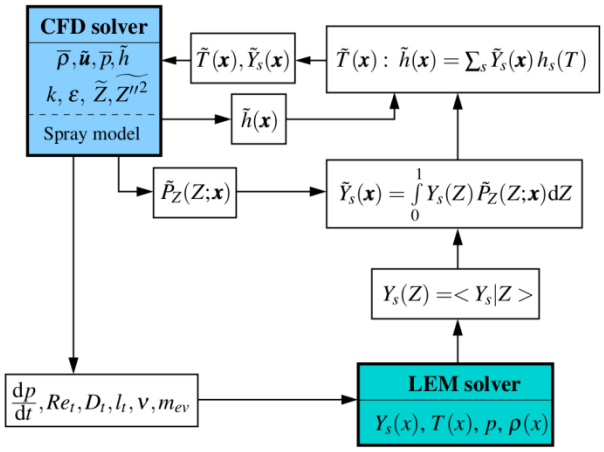

Figure 1: The code structure of the RILEM

Fuel mapping strategy

For a consistent representation of the fuel injection and evaporation process during the 3D CFD simulation on the LEM domain, i.e. a representative fuel distribution and a consistent global equivalence ratio, we propose the following strategy: First the total evaporated mass m_{evap}^{CFD} in the CFD domain is calculated:

$$(7)\quad m_{evap}^{CFD} = \sum_{i=1}^{n_{evap}} \dot{\rho}_{evap,i}^{CFD} \cdot V_{evap,i} \cdot dt$$

where $\dot{\rho}_{evap,i}^{CFD}$ is the evaporated fuel mass per volume in CFD cell i, $V_{evap,i}$ is the corresponding cell volume and n_{evap} the number of cells with positive evaporation rates. The ratio of the total volume of fuel cells with positive evaporation rates to the total volume of the CFD domain α is

$$(8)\quad \alpha = \frac{\sum_{i=1}^{n_{evap}} V_{evap,i}}{V^{CFD}}$$

in which V^{CFD} is the volume of the whole CFD domain.

On the LEM line fuel should be injected representative of the fuel injection process on the CFD side. As mentioned above, we are using a spherical formulation of the LEM. In a spherical formulation the LEM line can be interpreted as a line of sight through the center of a sphere. However, we do not assume spherical symmetry here and allow turbulent eddies across the center of the sphere. The domain size of the LEM is the same as the CFD domain size: $V^{CFD} = V^{LEM}$, leading to

$$(9)\quad r^{LEM} = \left(\frac{3}{4}\frac{V^{LEM}}{\pi}\right)^{\frac{1}{3}}.$$

We place the origin of the spherical coordinate system in the middle of the LEM domain, which ranges from $r \in [-r^{LEM}, r^{LEM}]$.

The fuel is distributed on a fraction of the LEM domain in the middle of the LEM line. The length of that fraction r_{evap}^{LEM} is chosen to be:

$$(10)\, r_{evap}^{LEM} = \left(\frac{3}{4}\frac{V^{LEM} * \alpha}{\pi}\right)^{\frac{1}{3}}$$

There is a certain number of cells within the radius r_{evap}^{LEM}. Assuming that the spatial distribution of fuel evaporated during Δt is distributed equally to all LEM cells n_{evap}^{LEM}, the amount of fuel inserted in each LEM $n_{evap,i}^{LEM}$ is

$$(11)\, m_{evap,i}^{LEM} = \frac{m_{evap}^{CFD}}{n_{evap}^{LEM}}$$

Chemical mechanism

The chemical reaction mechanism for n-heptane combustion used in this work is the reduced mechanism of Maroteaux and Noel [6], consisting of 26 chemical reactions with 25 species. This mechanism is able to predict ignition delay times and heat release rates under conditions relevant to engine applications. The formation of pollutants is not taken into account.

Results and Discussion

To demonstrate the performance of the newly developed model in combination with the novel fuel mapping strategy, a numerical simulation for a high pressure high temperature spray combustion chamber was performed. The case examined has previously been investigated [25]. High pressure high temperature combustion chambers are alternatives to conventional combustion chambers and developed to investigate sprays under engine-like conditions.

The size of the computational domain is 1 cm x 1cm x 10 cm. The nozzle is located in the middle of the chamber at the upper wall and has a diameter of 0.19 mm. The chamber is fueled with an n-heptane spray. The CFD simulations were carried out using OpenFOAM 2.0.x with a 41 x 41 x 100 grid containing 178164 gridpoints over the entire three-dimensional domain. Adiabatic wall boundary conditions were set, with zero gradient conditions for all dependent variables. All simulations were conducted in serial mode on an Intel Xeon CPU with 2.0 GHZ. The required time for the computation was about 3 days with a LEM of 4000-11000 gridpoints on average (due to the change of turbulent length scales in particular and the adaptive mesh refinement in the LEM code the number of gridpoints varies over time). The computational time on the LEM side is very dependent on the grid size and the chosen chemical mechanism, and can therefore be reduced by scaling down the LEM line or using a simpler chemical mechanism. The initial conditions were 800 K for the temperature of the air in the chamber and 42 bar pressure. The injected mass of fuel is 6 mg. Periodic boundary conditions are used on the LEM line.

Comparison with Experiments

The numerical results of combustion behavior obtained using RILEM depend strongly on the distribution of the mixture fraction $\tilde{Z}$ and the mixture

fraction variance $\widetilde{Z''^2}$ because these variables are used to specify the mixture fraction PDF that is used to compute Favre-averaged mass fraction values. The mapping of the representative LEM solution onto physical space in the CFD domain alone is responsible for time-dependent vapor penetration depth, as shown in Fig. 2. Both of the values, mixture fraction and its variance, depend on the rate of fuel evaporation, which is an outcome of the CFD spray model. To evaluate the performance of the spray model, the vapor penetration depth, which is defined as the distance between the nozzle and the most distant point at which the fuel vapor mass fraction is greater than five per cent, is a usually considered result. The agreement between the calculated penetration depth and the analytical solution reported by Wakuri et al. [26], who based their derivation on the conservation of momentum and assumed that the depth of penetration is proportional to $t^{1/2}$, is quite reasonable here in this case and can be observed fig. 2.

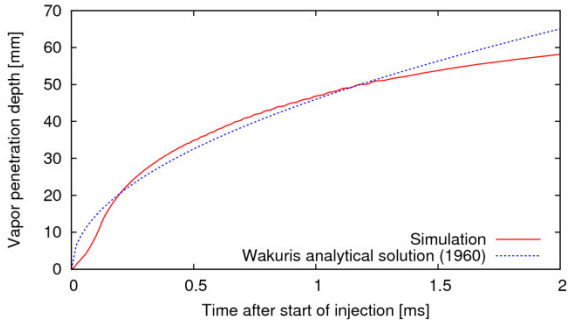

Figure 2: Vapor penetration depth

The predicted ignition delay time under the studied conditions is about 1.3 ms. Koss et al. [13] perfomed experiments in a spray vessel and obtained ignition delay times around 1.6 ms. In [25] Pitsch et al. calculated a 1.5 ms ignition delay with a flamelet model. In the future, the new model will be used to investigate the effects of mixture inhomogeneity on ignition delay. To demonstrate the qualitative performance of the RILEM model, comparisons between the RILEM and RIF model for the temperature and mixture fraction development over time on the CFD domain are shown in Figures 3 and 4. It should be noted that the spray evaporation and breakup models for the RILEM and the RIF model are not the same, leading to qualitatively different mixture fraction distributions within the CFD domain. In addition Figures 5 and 6 present some species mass fractions over mixture fraction space of the LEM at different times of the computation.

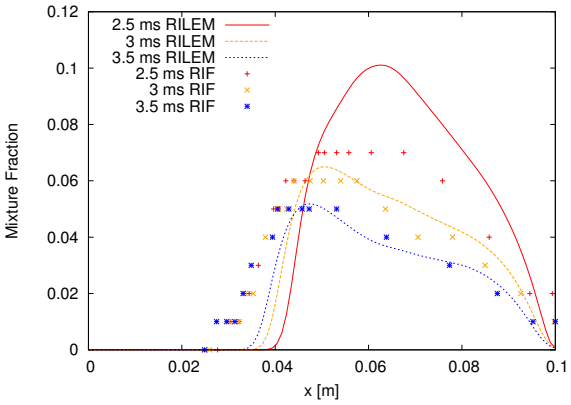

Figure 3: Comparison between interpolated values of the mixture fraction on a line running along the length of the simulated combustion chamber and results from Pitsch et al [25] within the CFD domain at t = 2.5, 3, 3.5 ms. On the horizontal axis of the plot, 0 corresponds to a position at the bottom of the chamber and a value of 0.1 corresponds to a position immediately below the nozzle.

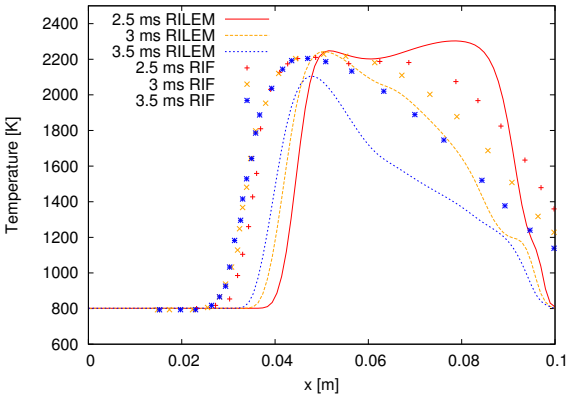

Figure 4: Comparison between interpolated values of the temperature on a line running along the length of the simulated combustion chamber and results from Pitsch et al [25] within the CFD domain at t = 2.5, 3, 3.5 ms. On the horizontal axis of the plot, 0 corresponds to a position at the bottom of the chamber and a value of 0.1 corresponds to a position immediately below the nozzle.

Due to a different spray models Fig. 3 shows some qualitative and quantitative differences in the mixture fraction distribution over time between the RILEM and the RIF model. Directly at the nozzle, x = 0.1 m in Fig. 3, the RIF model shows already a non-zero mixture fraction value, indicating that there are already small enough droplets to evaporate. In the RILEM simulation, big droplets are leaving the nozzle which need to break up first before they are able to evaporate. Further down it is obvious that the spray penetrates further in the CFD domain in the RIF model. Nevertheless the mixture fraction distribution looks quite similar for 3 and 3.5 ms.
Fig. 4 shows the corresponding temperatures for the mixture fractions of Fig. 3. Directly at the nozzle the

temperature for the RILEM corresponds to the ambient air temperature because the mixture fraction in the gas phase is zero. Further downstream the nozzle until x = 0.06 m the temperature distribution is different due to different droplet evaporation and break up in the RILEM and the RIF model. At x = 0.047 m the mixture fraction and the temperature match reasonably well at 2.5 and 3 ms. At 3.5 ms the mixture fraction goes down for both simulations as the mixture within the CFD domain leans out. The RILEM simulation shows overall lower temperatures at 3.5 ms compared to the RIF model. At x = 0.047 the maximum temperature for RIF does not change at all in contrast to RILEM, which yields a smaller maximum temperature of 2050 K instead of 2200 K. Further and more detailed comparisons between our RILEM approach and RIF models will be presented in a forthcoming publication.

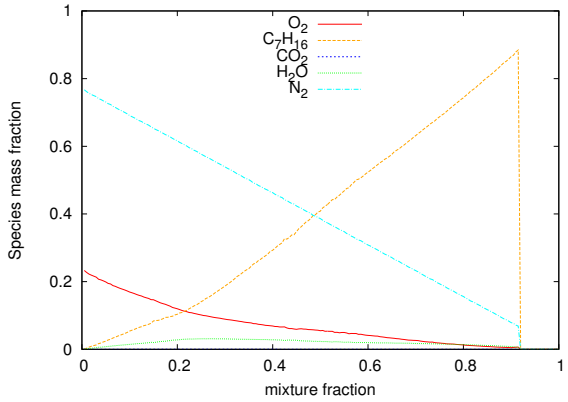

Figure 5: Mass fractions of individual chemical species within the mixture fraction space of the LEM at = 0.5 ms

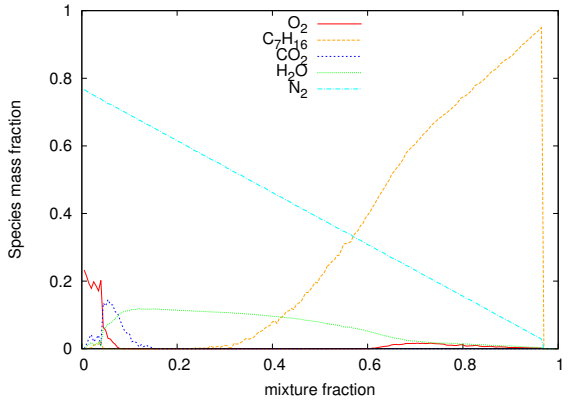

Figure 6: Mass fractions of individual chemical species within the mixture fraction space of the LEM at = 2.5 ms

Figs. 5 and 6 show the major species mass fractions on the LEM side before and after combustion at t = 0.5 ms and t = 2.5 ms. The species mass fractions shown here are conventional ensemble averages over the different states along the LEM line at constant mixture fraction value. These different states for identical mixture fraction values can be interpreted as effects of the fluctuating time history of the scalar dissipation rate within the LEM. The profiles in this case are quite smooth indicating that the LEM line is long enough so that the statistical fluctuations in the scalar dissipation rate are captured. The statistical properties of the RILEM will be examined in future studies.

As expected for the investigated conditions, the species mass fraction profiles are very similar to flamelet profiles. There are some small wrinkles in the profiles which are due to turbulent eddies interacting with the flame on the LEM line.

In the unburnt state after 0.5 ms of the simulation time there is no conversion into CO_2 but already a bit of conversion into water due to low temperature chemistry over the whole mixture fraction space. Almost all oxygen is still available.

For the burning case Fig. 6, it is obvious that the highest temperature is where the CO_2 peak occurs near stoichiometric conditions at a mixture fraction value around 0.06. The oxygen goes to zero from that point up to a mixture fraction of 0.6, indicating full conversion of the available oxygen.

Summary/Conclusions

In the present study a new model for turbulent non-premixed combustion based on the linear eddy model has been developed. Regime-independent combustion modeling is achieved by using a representative linear eddy model (LEM), which enables regime-independence because it includes the local impact of the turbulent motion of the flow on the chemistry of combustion. The representative LEM is solved concurrently with the advancement of the CFD simulation and ensures a direct interaction between the evolving flow solution on the CFD side and the combustion process resolved at all length and time scales along the one-dimensional LEM line. In addition a consistent fuel mapping strategy based on a spherical implementation of the LEM is used here. As a qualitative test the new model was applied to a high pressure, high temperature spray combustion process involving n-heptane. Promisingly, the fuel mapping strategy enables a consistent mapping of the CFD domain status at all times of the realization, the predicted ignition delay times and temperatures are in reasonably good agreement with previously obtained results. Unsurprisingly, given that RILEM is a new model, there are several open questions that remain to be answered. In particular, it will be necessary to study the model's statistical properties such as the variation in the scalar dissipation rate. Furthermore, many improvements of the model can be envisaged, some of which could be realized by using techniques that have been fruitful with flamelet approaches. For example, like in RIF models, it should be straightforward to use multiple representative LEMs instead of one single LEM. In addition, the model will be validated by comparing its output to that of existing models and experimental data.

References

1. Kerstein, A. R., J. Fluid Mech. 392, 277–334, 1999.
2. Lignell, D. O., Kerstein, A. R., Sun, G., Monson, E. I., Theor. Comput. Fluid Dyn., Vol. 27, Issue 3-4, pp 273-295, 2013.
3. Kösters, A., Golovitchev, V., Karlsson, A., SAE Int.J.Fuel and Lubricants 5(2), 2012.
4. Smith, T. M., Menon, S., Combustion Science and Technology, 128, 99-130, 1997
5.Goodwin, D.: Cantera, http://code/google.com/p/cantera
6. Maroteaux F., Noel L., Combustion and Flame, 146, 246-267, 2006.
7. Echekki, T., pages 177-192. Springer, 2011.
8. El-Asrag, H., and Menon, S., Combustion and Flame, 156:385-395,2009.
9. El-Asrag, H., Lu, T., Law, C. K., and Menon, S., Combustion and Flame, 150:108-126, 2007.
10. Kerstein, A. R., Combustion Science and Technology, 60:391-421, 1988.
11. Kerstein, A.R., Combustion and Flame, 75:397-413, 1989.
12. Kerstein, A.R., Journal of Fluid dynamics, 240:289-313, 1992.
13. Koss, H. J., Brueggemann, D. Additional report, IDEA. 1992
14. Kerstein, A.R., Combustion Science and Technology, 81:75-96, 1992.
15. Klein, R., Introduction to Turbulent Combustion, Brussels, Belgium, January 6-9, 1999. Von Karman Institute for Fluid Dynamics.
16. Meyer, D. W., and Jenny, P., Physics of Fluids, 18:035105, 2006.
17. Oevermann, M., Schmidt, H., and Kerstein, A. R., Combustion and Flame, 155:370-379, 2008.
18. Patel, N., and Menon, S., Combustion and Flame, 155:228-257, 2008.
19. Pitsch, H., Chen, M., and Peters, N., Proceedings of the Combustion Institute, p. 1057-1064, 1998.
20. Sankaran, V., and Menon, S., In Proceedings of the Combustion Institute, 30:575-582, 2005.
21. Sen, B. A., Combustion and Flame, 157:62-74, 2010.
22. Sen, B. A., and Menon, S., Combustion and Flame, 157:566-578, 2010.
23. Some, K., and Menon, S., Journal of Engineering for Gas Turbines and Power, 125:435-443, 2003
24. Steeper, R., Sankaran, V., and Oefelein, J., SAE Technical Paper Series, 2007-01-4131, 2007.
25. Pitsch, H., Wan, Y. P., and Peters, N., SAE Technical Paper 952357, 1995.
26. Wakuri, Y., Fujii, Amitani, M., T., Tsuneya, R., Bulletin of J.S.M.E., Vol.3, No. 9, 1960.
27. Ciezki, H. K., Adomeit, G., Combustion and Flame, 93: 421-433, 1993.
28. Oevermann, M., Schmidt, H., Kerstein, A. R., Combustion and Flame, 155:370-379, 2008.
29. Schrödinger, C., Paschereit, C. O., Oevermann, M., Combustion Science and Technology, 186:1392-1409, 2014.
30. Lackmann, T., Kerstein A. R., Oevermann, M., SAE Technical Paper Series, 2015.
31. Koss, H. J., Brueggemann, D. Additional report, IDEA. 1992.